The Astrophysical Journal, 942:18 (10pp), 2023 January 1 https://doi.org/10.3847/1538-4357/aca01f

Implications of the Milky Way Travel Velocity for Dynamical Mass Estimates of the Local Group

Katie Chamberlain[1,2], Adrian M. Price-Whelan[2], Gurtina Besla[1], Emily C. Cunningham[2], Nicolás Garavito-Camargo[2], Jorge Peñarrubia[3], and Michael S. Petersen[4]
[1] University of Arizona, 933 N. Cherry Avenue, Tucson, AZ 85721, USA
[2] Center for Computational Astrophysics, Flatiron Institute, Simons Foundation, 162 Fifth Avenue, New York, NY 10010, USA
[3] Institute for Astronomy, University of Edinburgh, Royal Observatory, Blackford Hill, Edinburgh, EH9 3HJ, UK
[4] Institut d'Astrophysique de Paris, 98 Bis Blvd Arago, F-75014 Paris, France
Received 2022 April 14; revised 2022 October 13; accepted 2022 November 2; published 2022 December 29

Abstract

The total mass of the Local Group (LG) is a fundamental quantity that enables interpreting the orbits of its constituent galaxies and placing the LG in a cosmological context. One of the few methods that allows inferring the total mass directly is the "Timing Argument," which models the relative orbit of the Milky Way (MW) and M31 in equilibrium. The MW itself is not in equilibrium, a byproduct of its merger history and including the recent pericentric passage of the Large Magellanic Cloud (LMC), and recent work has found that the MW disk is moving with a lower bound "travel velocity" of $\sim$32 km s^{-1} with respect to the outer stellar halo. Previous Timing Argument measurements have attempted to account for this nonequilibrium state, but have been restricted to theoretical predictions for the impact of the LMC specifically. In this paper, we quantify the impact of a travel velocity on recovered LG mass estimates using several different compilations of recent kinematic measurements of M31. We find that incorporating the measured value of the travel velocity lowers the inferred LG mass by 10%–12% compared to a static MW halo. Measurements of the travel velocity with more distant tracers could yield even larger values, which would further decrease the inferred LG mass. Therefore, the newly measured travel velocity directly implies a lower LG mass than from a model with a static MW halo and must be considered in future dynamical studies of the Local Volume.

Unified Astronomy Thesaurus concepts: Local Group (929); Andromeda Galaxy (39); Magellanic Clouds (990); Milky Way Galaxy (1054); Triangulum Galaxy (1712); Keplerian orbit (884); Orbital motion (1179)

1. Introduction

The total mass of the Local Group (LG) is an important quantity in many local cosmological and Milky Way (MW) applications. For example, it is used to identify analogous halos in cosmological simulations and thus allows comparing host galaxy and satellite galaxy number counts and properties (e.g., Dooley et al. 2017; Marinacci et al. 2017; Patel et al. 2017b; Besla et al. 2018; Patel et al. 2018; Garrison-Kimmel et al. 2019a, 2019b; Sawala et al. 2022). It is also used to turn the kinematics of LG galaxies into orbital histories (e.g., Peebles 2017), which is used to interpret their gas content (e.g., Fillingham et al. 2018; Putman et al. 2021) and star formation histories (e.g., Tolstoy et al. 2009). However, as most of the mass in the LG is in dark matter distributed over megaparsec scales, it is difficult to directly measure its total mass.

Given its utility in studies of the local universe, several methods have been used to dynamically infer the mass of the LG. Many of these techniques determine the individual masses of the MW and M31 independently (e.g., Watkins et al. 2010; Fardal et al. 2013; Diaz et al. 2014; Carlesi et al. 2017; Patel et al. 2018; Eadie & Jurić 2019; Fritz et al. 2020; Deason et al. 2021; Villanueva-Domingo et al. 2021; Wang et al. 2022), often via the dynamics of their satellites and stellar streams, then combine them to get an estimate of the total LG mass. However, these methods generally only measure the enclosed mass of the MW or M31 within some internal radius (i.e., much smaller than LG scales) and then extrapolate, leading to mass-profile-dependent estimates of the total LG mass. Other techniques aim to more directly measure the mass of the LG en masse, for example looking for LG analogs in cosmological simulations based on stellar mass and kinematic criteria (e.g., Li & White 2008; González et al. 2014; Zhai et al. 2020; Hartl & Strigari 2022), by studying the kinematics of Local Volume (LV) galaxies (e.g., Diaz et al. 2014; Peñarrubia et al. 2014), or by applying machine-learning (ML) techniques to hydrodynamic simulation data (e.g., McLeod et al. 2017; Villanueva-Domingo et al. 2021). One of the earliest methods utilized in this vein is the "Timing Argument," which uses the fact that the LG galaxies (most often the MW and M31) are bound and approaching pericenter in their relative orbit, but must have been close enough over cosmic time to not be pulled apart by the Hubble flow. The Timing Argument can be generalized to simultaneously model the orbits of LV galaxies around the LG (Peñarrubia et al. 2016; Peñarrubia & Fattahi 2017), but here we restrict our analysis to the "classic" Timing Argument using only the MW and M31. We summarize the relevant details of the Timing Argument method in Section 2.1.

The Timing Argument (using the MW and M31) uses the observed kinematics of M31 to model the relative orbit of the two galaxies as a Keplerian orbit. Assuming Keplerian dynamics enables dynamically measuring the total mass of the MW and M31 with analytic expressions for all relevant kinematic quantities because of the simplicity of the two-body equations of motion. The inferred mass from the Timing

Argument thus directly depends on the observationally measured kinematics of the M31 center.

However, the LG is not in equilibrium. In the past decade, a number of studies have begun to consider of the impact of the Large Magellanic Cloud (LMC) on the mass and inferred dynamics of the LG. Peñarrubia et al. (2016) studied the effect of the presence of the LMC on the total mass estimates of the LG via the Timing Argument by modelling the motion of M31 about the MW–LMC barycenter, and using the kinematics of 35 LV galaxies to simultaneously measure a MW mass of $M_{\rm MW} = 1.04^{+0.26}_{-0.23} \times 10^{12} M_{\odot}$, M31 mass of $M_{\rm M31} = 1.33^{+0.39}_{-0.33} \times 10^{12} M_{\odot}$, LMC mass of $M_{\rm LMC} = 0.25^{+0.09}_{-0.08} \times 10^{12} M_{\odot}$, and LG mass of $M_{\rm LG} = 2.64^{+0.42}_{-0.38} \times 10^{12} M_{\odot}$. Another recent Timing Argument work by Benisty et al. (2022) modeled the orbital history of M31 and the MW, with and without a mass and orbital model of the LMC, to estimate the contribution of the LMC-induced shift in the MW barycenter on the measured tangential and radial velocities of M31, then applied these corrections to their model to remove the impact of the LMC in their analysis, and found that the inferred LG mass decreased by 10%.

Recent studies of the dynamics of the MW and its satellites have revealed that the infall of the Magellanic Clouds (MCs) is causing significant distortions to the dark matter and stellar distribution in the MW halo (Laporte et al. 2018a, 2018b; Garavito-Camargo et al. 2019; Conroy et al. 2021; Erkal et al. 2021). In addition, numerous studies of the interaction between the MW and LMC (using simulated analogs) have quantified the expected LMC-induced reflex motion of the MW disk and inner halo, which are likely being accelerated away from the center-of-mass reference frame of a static MW halo (Gómez et al. 2015; Cunningham et al. 2020; Petersen & Peñarrubia 2020; Garavito-Camargo et al. 2021). The induced systematic shift in the measurements of the M31 kinematics may have created a bias in previous mass measurements via the Timing Argument, thus impacting interpretations of LG dynamics, orbital histories, cosmological context, etc.

Previous Timing Argument studies have accounted for the impact of an LMC-induced reflex motion on the orbital histories of the other galaxies in the LG. However, other satellite mergers, such as the ongoing merger with the Sagittarius dwarf galaxy, as well as the past merger with the progenitor of the Gaia–Enceladus–Sausage, have likely also imparted their own reflex motion to the inner MW halo. A signature of the reflex motion of the MW is imprinted as a velocity dipole in the radial velocities of stars in the outer stellar halo (Garavito-Camargo et al. 2021). Recently, the instantaneous velocity offset of the inner MW with respect to the outer halo was directly measured using tracer stars in the stellar halo of the MW (the "travel velocity"; Petersen & Peñarrubia 2021). Thus, the newly measured travel velocity can be used in Timing Argument studies in place of orbital modeling to account for the expected perturbations of the inner MW halo without having to make assumptions about the mass or dynamical history of the LMC or other satellites.

Studies have considered variations to the standard Timing Argument model. For example, one such model considered the effect of dark energy, and finds that the addition of a cosmological constant to the energy equations yields a ∼13% increase in the recovered mass (Partridge et al. 2013). Similarly, the travel velocity of the MW disk, which has only recently been first measured, introduces its own complication to the standard Timing Argument model.

In this article, we quantify the impact of this newly measured MW disk motion on LG mass measurements using the timing argument, thus accounting for observational misinterpretations in a model-independent way for the first time. We also show that improvements in the measurements of the MW travel velocity may lead to even larger discrepancies between TA schemes with and without a MW travel velocity. We also explore a combination of recent measurements of the distance and proper motions of M31 to infer the effect of the travel velocity in a data-set-independent way. As a result, we find that the travel velocity significantly impacts the inferred mass of the LG in Timing Argument studies, and thus must be accounted for in further dynamical studies of the LV.

2. Methods and Data

2.1. Dynamical Model: The Timing Argument

Following past work that utilizes the "Timing Argument," we assume that the orbital trajectories of the MW and M31—the LG system—over cosmic history are well described by Keplerian orbits (e.g., Kahn & Woltjer 1959; Lynden-Bell 1981; Kroeker & Carlberg 1991; Li & White 2008; van der Marel et al. 2012; Peñarrubia et al. 2016). By assuming that M31 and the MW are gravitationally bound and were last at closest approach in the early universe (i.e., the two galaxies have not yet strongly interacted), we can then use the present-day kinematics of M31 relative to the MW to estimate the total mass of the LG (i.e., using the Timing Argument).

In this work, we largely follow the methodology and notation defined in Peñarrubia et al. (2016). Briefly recapping the classical Timing Argument method, we assume that the dynamics of the MW and M31 pair is dominated by the local gravitational potential of the LG, and therefore the Hubble flow can be neglected for computing the relative orbits of the galaxies (see, e.g., Peñarrubia et al. 2014). Since we observe the relative position and motion between M31 and the MW, we reduce the dynamics of the galaxies in the LG system to a single Keplerian orbit that specifies the relative orbit between the galaxies and is completely determined by four model parameters: the total mass of the LG, $M_{\rm LG}$, the semimajor axis, a, the eccentricity, e, and the present value of the eccentric anomaly, η.

In terms of these four model parameters, the closed-form equations for relevant two-body quantities that are closer to observables, like the separation between the masses, r, the elapsed time since last pericenter, t, and the radial and tangential velocity components, $v_{\rm rad}$ and $v_{\rm tan}$, are given by

$$r = a\,(1 - e\cos\eta), \tag{1}$$

$$t = \left(\frac{a^3}{GM}\right)^{1/2}(\eta - e\sin\eta), \tag{2}$$

$$v_{\rm rad} = \left(\frac{GM}{a}\right)^{1/2}\frac{e\sin\eta}{1 - e\cos\eta}, \tag{3}$$

$$v_{\rm tan} = \left(\frac{GM}{a}\right)^{1/2}\frac{\sqrt{1 - e^2}}{1 - e\cos\eta}. \tag{4}$$

In the expressions above, r is the separation between the centers of the MW and M31 halos, the time since last pericenter, t, is the age of the universe, and the velocity

components, ($v_{\rm rad}$, $v_{\rm tan}$), express the radial and tangential velocity components of M31 relative to the center of the MW halo.

In a simpler universe where the MW and M31 are point masses and there are no other massive bodies in the LG system, we could transform the observed heliocentric sky position, distance, and velocity of M31 to a MW Galactocentric reference frame and combine these with an estimate of the Hubble time to obtain the four "observables" (r, t, $v_{\rm rad}$, $v_{\rm tan}$). These observables would be enough to infer the four model parameters ($M_{\rm LG}$, a, e, η) using Equations (1)–(4).

To describe this "classical" Timing Argument approach in more detail and set the stage for extending it, we adopt the notation of Peñarrubia et al. (2016) in which $\boldsymbol{v}_{\rm A\to B}$ represents the velocity vector of A as measured in the reference frame of B and $\boldsymbol{x}_{\rm A\to B}$ represents the position vector of A as measured from B. With this notation, $\boldsymbol{v}_{\rm A\to B} = -\boldsymbol{v}_{\rm B\to A}$ and $\boldsymbol{v}_{\rm A\to C} = \boldsymbol{v}_{\rm A\to B} + \boldsymbol{v}_{\rm B\to C}$.

In the classical Timing Argument, the MW disk and M31 are assumed to occupy the center of the potential well of their dark matter halos and have zero velocity with respect to the halos. We refer to this reference frame in the MW dark matter halo as $\rm MW_{halo}$. Thus, the position and velocity of M31 with respect to the MW can be represented by $\boldsymbol{x}_{\rm M31\to MW_{halo}}$ and $\boldsymbol{v}_{\rm M31\to MW_{halo}}$, which are assumed to be equivalent to the position and velocity of M31 with respect to the center of the MW disk. Then, the *observed* position and velocity of M31, measured in a heliocentric reference frame, are given by

$$\boldsymbol{x}_{\rm M31\to\odot} = \boldsymbol{x}_{\rm M31\to MW_{halo}} + \boldsymbol{x}_{\rm MW_{halo}\to\odot}, \quad (5)$$

$$\boldsymbol{v}_{\rm M31\to\odot} = \boldsymbol{v}_{\rm M31\to MW_{halo}} + \boldsymbol{v}_{\rm MW_{halo}\to\odot}. \quad (6)$$

Here $|\boldsymbol{x}_{\rm M31\to MW_{halo}}| = r$ as determined from Equation (1), $\boldsymbol{v}_{\rm M31\to MW_{halo}}$ is determined completely by the Keplerian model parameters (through $v_{\rm rad}$ and $v_{\rm tan}$), and the position and velocity of the center of the MW halo as measured from the Sun are $\boldsymbol{x}_{\rm MW_{halo}\to\odot}$ and $\boldsymbol{v}_{\rm MW_{halo}\to\odot}$.

However, the true dynamics of the MW–M31 system are not so simple. Perturbations introduced by interactions and mergers between the MW and its satellite galaxies, such as the merger of the Sagittarius dwarf galaxy or the recent pericentric passage of the LMC, break the assumption that the MW disk is stationary in the center of its dark matter halo. In fact, these interactions will introduce an additional reflex motion component in observations from the MW disk compared to the $\rm MW_{halo}$ reference frame. The LMC's impact on the dynamics of the MW disk and inner halo have been studied in detail by, e.g., Gómez et al. (2015), Garavito-Camargo et al. (2019, 2021), and Petersen & Peñarrubia (2020). These works imply that we must include additional terms in Equations (5) and (6) to account for the travel velocity of the MW disk with respect to the center of the halo in its unperturbed state. Thus, the observed position and velocity vectors of M31 from the solar reference frame become

$$\boldsymbol{x}_{\rm M31\to\odot} = \boldsymbol{x}_{\rm M31\to MW_{halo}} + \boldsymbol{x}_{\rm MW_{halo}\to MW_{disk}} + \boldsymbol{x}_{\rm MW_{disk}\to\odot}, \quad (7)$$

$$\boldsymbol{v}_{\rm M31\to\odot} = \boldsymbol{v}_{\rm M31\to MW_{halo}} + \boldsymbol{v}_{\rm MW_{halo}\to MW_{disk}} + \boldsymbol{v}_{\rm MW_{disk}\to\odot}, \quad (8)$$

where $\rm MW_{halo}$ refers to a reference frame centered at and moving with the center of mass of the outer MW halo, $\rm MW_{disk}$ refers to a reference frame centered at and moving with the center of the MW disk, and $\boldsymbol{x}_{\rm MW_{disk}\to\odot}$ and $\boldsymbol{v}_{\rm MW_{disk}\to\odot}$, respectively, are the adopted solar position and velocity in the Galaxy. The values we adopt for $\boldsymbol{x}_{\rm MW_{disk}\to\odot}$ and $\boldsymbol{v}_{\rm MW_{disk}\to\odot}$ (shortened to $\boldsymbol{x}_\odot$ and $\boldsymbol{v}_\odot$) are given in Table 1 below.[5]

Table 1
Observational Datasets Used for Comparison Throughout Analysis and Their References

	vdMG08 Dist. + HST PM	Cepheid Dist. + Gaia PM	Cepheid Dist. + HST PM
D (kpc)	770 ± 40[a]	761 ± 11 kpc[f]	761 ± 11[f]
$v_{\rm rad}$ (km s^{-1})	-301 ± 1[b]	-301 ± 1[b]	-301 ± 1[b]
μ_{α^*} (μas yr^{-1})	34.30 ± 8.25[c]	48.98 ± 10.47[g]	34.30 ± 8.25[c]
μ_δ (μas yr^{-1})	-20.22 ± 7.71[c]	-36.85 ± 8.03[g]	-20.22 ± 7.71[c]
$\boldsymbol{x}_\odot$ (kpc)	$(-8.29,0,0)$[d]	$(-8.122, 0, 20.8)$[h]	$(-8.122, 0, 20.8)$[h]
$\boldsymbol{v}_\odot$ (km s^{-1})	$(11.1, 251.54, 7.25)$[d]	$(12.9, 245.6, 7.78)$[i]	$(12.9, 245.6, 7.78)$[i]
$t_{\rm peri}$ (Gyr)	13.75 ± 0.11[e]	13.801 ± 0.024[j]	13.801 ± 0.024[j]

Note. Each value is measured for M31 with respect to the Sun. D is the distance, $v_{\rm rad}$ is the radial velocity, and (μ_α^*, μ_δ) are proper motions in R.A. cosdec and Decl. $\boldsymbol{x}_\odot = (x, y, z)$ and $\boldsymbol{v}_\odot = (U_{\rm pec}, V_{\rm pec} + V_0, W_{\rm pec})$ are the the position of the Sun and the solar motion with respect to the Galactic center, with the x-axis pointing from the projection of the Sun on the disk toward the Galactic center, and the z-axis pointing in the direction of the North Galactic pole. $t_{\rm peri}$ is the time elapsed since the last pericenter of the M31 Keplerian orbit, which in this case is the age of the universe.

References. (a) van der Marel & Guhathakurta (2008); (b) Courteau & van den Bergh (1999); (c) van der Marel et al. (2012); (d) Schönrich et al. (2010), McMillan (2011); (e) Jarosik et al. (2011); (f) Li et al. (2021); (g) Salomon et al. (2021); (h) Gravity Collaboration et al. (2018), Bennett & Bovy (2019); (i) Drimmel & Poggio (2018); (j) Planck Collaboration et al. (2020).

Observationally, the reflex motion of the disk imprints itself on velocity measurements as an instantaneous velocity shift. Recently, Petersen & Peñarrubia (2021) used tracers in the outer MW stellar halo to measure this instantaneous travel velocity $\boldsymbol{v}_{\rm travel} = \boldsymbol{v}_{\rm MW_{halo}\to MW_{disk}}$. They find $|\boldsymbol{v}_{\rm travel}| = 32 \pm 4$ km s^{-1} with a highest likelihood apex direction in Galactocentric coordinates of $(\ell, b)_{\rm apex} = (56^{+9}_{-9}, -34^{+10}_{-9})$ degrees. We assume that $\boldsymbol{x}_{\rm MW_{halo}\to MW_{disk}} \approx 0$ motivated by the fact that this displacement is likely much smaller than the distance between the MW and M31 $\boldsymbol{x}_{\rm MW_{halo}\to MW_{disk}} \ll r$ (as expected from simulations; e.g., Garavito-Camargo et al. 2021). However, it is important to note that this displacement is still significant on scales relevant for many other MW studies (see Section 4.3 for more details).

Figure 1 shows a schematic of these different vectors—all drawn in a frame that is comoving with the $\rm MW_{halo}$ frame—and a rough illustration of the geometry we assume. For clarity, we show $\boldsymbol{x}_{\rm MW_{halo}\to MW_{disk}} = \boldsymbol{x}_{\rm travel}$, $\boldsymbol{v}_{\rm MW_{halo}\to MW_{disk}} = \boldsymbol{v}_{\rm travel}$, and $\boldsymbol{v}_{\rm M31\to\odot} = \boldsymbol{v}_{\rm obs}$.

2.2. Data Sets

The present distance and relative velocity of M31, as well as the age of the universe (used in Equation (2)), are key observables that are used to constrain our Timing Argument model. In this paper, we consider three different compilations of data to understand how different measurements might affect the Timing Argument model with the addition of the travel velocity. In particular, we consider two different M31 distance measures:

[5] Note that, in principle, there is also a term $\boldsymbol{v}_{\rm M31_{halo}\to M31_{disk}}$; however, there are not yet measurements of the differential motion of the M31 disk with respect to the M31 halo, so we neglect this term. See further discussion in Section 4.5.

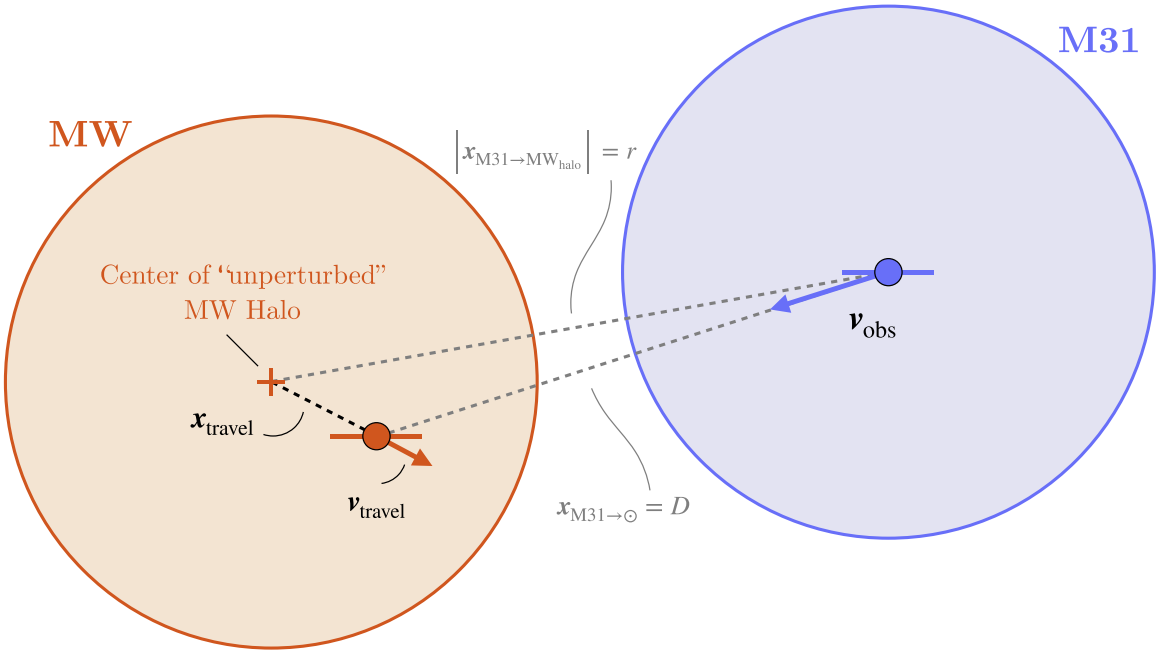

Figure 1. Schematic of the Milky Way (MW) and M31 system, not to scale. The shaded regions represent the halos of both galaxies. Shown are an artistic representation of the velocity and position vectors that are relevant in our model, including $D = \boldsymbol{x}_{M31\to\odot}$, the measured distance to M31, $\boldsymbol{x}_{M31\to MW_{halo}}$, the distance between the centers of both halos, and $\boldsymbol{v}_{obs}$, the measured 3D velocity of M31. Finally, $\boldsymbol{x}_{travel}$ and $\boldsymbol{v}_{travel}$ are the present distance and velocity between the center of the MW halo and the center of the MW disk. For this study, we assume $\boldsymbol{x}_{travel} \ll r$, D, and $|\boldsymbol{v}_{travel}| = 32 \pm 4$ km s^{-1} from Petersen & Peñarrubia (2021).

an approximated distance measure from van der Marel & Guhathakurta (2008), and a more accurate Cepheid-based distance measure from Li et al. (2021). We also consider two different M31 proper-motion measurements: Hubble Space Telescope (HST)-based proper motions from van der Marel et al. (2012), and a more recent Gaia early Data Release 3 (eDR3)-based proper-motion measure from Salomon et al. (2021).

We have split these measurements into three compiled data sets:

1. vdMG08 Dist. + HST PM: the M31 distance measure from van der Marel & Guhathakurta (2008) and HST proper motions from van der Marel et al. (2012), the same data set as used to constrain the LG mass via the Timing Argument in van der Marel et al. (2012).
2. Cepheid Dist. + Gaia PM: a compilation of more recent M31 kinematic measurements, including a more precise Cepheid-based distance measure to M31 (Li et al. 2021) and updated Gaia eDR3 proper motions from Salomon et al. (2021).
3. Cepheid Dist. + HST PM: a hybrid data set with the Cepheid-based distance measure to M31 and the HST-based proper-motion measurement (Li et al. 2021; van der Marel et al. 2012).

The HST-based proper motions were originally presented in Sohn et al. (2012), and were then corrected for the internal kinematics and space motion of M31 in van der Marel et al. (2012), from which we used the "weighted average" heliocentric velocities in Table 4.[6] The Gaia-based M31 proper-motion measurement is slightly larger than the HST proper motion of M31, leading to an increased implied transverse velocity that, a priori, should lead to a higher inferred LG mass compared to the more radial orbit implied by the HST proper motions. See Table 1 for numerical values used in each of these data sets.

2.3. Bayesian Inference

We construct a likelihood function, $\mathcal{L}$, to quantify the probability of measuring the observed quantities $\boldsymbol{y} = \{D, v_{rad}, \mu_\alpha^*, \mu_\delta, t_{peri}\}$ given a timing argument model with parameters $\boldsymbol{\theta} = (M_{LG}, a, e, \eta, \alpha)$. Here, D is the distance to M31, v_{rad} is the radial velocity of M31, μ_α^* and μ_δ are the proper-motion components, and t_{peri} is the time since last pericenter. The parameter vector $\boldsymbol{\theta}$ contains M_{LG}, the total mass of the LG, a, the semimajor-axis, e, the eccentricity, η, the present value of the eccentric anomaly, and α, a nuisance parameter discussed in detail later in this section. We assume that the measurements are independent and have Gaussian uncertainties such that the likelihood function is a product:

$$\mathcal{L} = p(\boldsymbol{y}|\boldsymbol{\theta}) = \prod^{n} \frac{1}{\sqrt{2\pi}\,\sigma_n} \exp\left[-\frac{1}{2}\frac{(y_n - \tilde{y}_n(\boldsymbol{\theta}))^2}{2\sigma_n^2}\right], \quad (9)$$

where n indexes the elements of the data vector, σ_n is the corresponding uncertainty for the nth data element, and $\tilde{y}_n(\boldsymbol{\theta})$ is the model-predicted value for a given data component.

We then adopt prior probability distribution functions (pdfs) for the parameters and use these pdfs to compute the posterior pdf over the parameters given the data in order to generate samples from the posterior pdf using a Markov Chain Monte Carlo (MCMC) method. In order to recover the estimated mass distribution, we marginalize over all other model parameters.

In detail, we first use the four Timing Argument parameters to compute the present-day separation between the MW and

[6] Note that the referenced papers actually report velocity components and uncertainties. To transform from velocity back to proper motions, we divide out the adopted distance and deconvolve the distance uncertainty to obtain proper motions and uncertainties of $\mu_{\alpha^*} = 34.30 \pm 8.25$ mas yr^{-1} and $\mu_\delta = -20.22 \pm 7.71$ mas yr^{-1}.

Table 2
A Description of Our Adopted Prior Probability Distribution Functions Over the Timing Argument Model Parameters

Prior	Description
$M_{\rm LG}$: $\mathcal{N}_T(4.5, 3) \times 10^{12} M_\odot$	Mass of the Local Group
r: $\mathcal{N}_T(700, 100)$ kpc	Distance from M31 to $\rm MW_{disk}$
$\ln(1-e)$: $\mathcal{U}(-10, 0)$	Eccentricity (close to 1)
η: $\mathcal{U}(-\pi, \pi)$	Eccentric anomaly
α: $\mathcal{U}(-\pi, \pi)$	Position angle of M31 orbital plane from MW disk center

Note. Here, $\mathcal{U}(a, b)$ represents a uniform distribution over the domain (a, b), and $\mathcal{N}_T(\mu, \sigma)$ represents a truncated normal distribution with mean μ and standard deviation σ. We truncate the mass prior pdf to the range $(0.5, 20) \times 10^{12}\ M_\odot$ and the distance prior pdf to the range $(100, 10^4)$ kpc.

M31 halos and their relative radial and tangential velocities as defined in Equations (1)–(4). These velocity components represent the relative velocity M31 would have as observed from the center of an unperturbed MW halo. We then use the measured "travel velocity" of the MW disk, $\boldsymbol{v}_{\rm travel}$, to find the relative velocity of M31 with respect to the center of the moving MW disk (i.e., a moving MW Galactocentric frame). We finally transform from this Galactocentric frame to a heliocentric reference frame moving with the solar system barycenter (i.e., ICRS coordinates). At this final stage, we must introduce an additional nuisance parameter, α, that represents the orientation of the MW–M31 orbital plane as it intersects the tangent plane located at the sky position of M31 as viewed from the MW disk center. This parameter is needed to convert from the two-dimensional velocity components given by Equations (3)–(4) to the three-dimensional velocity components represented by the two proper-motion components and the radial velocity of M31. However, we stress that this position angle has no impact on the fundamental dynamical parameters and is only used for coordinate transformations.

We specify this model using the `Python` probabilistic programming package `pymc3` (Salvatier et al. 2016) and use the No-U-Turn Sampler (Homan & Gelman 2014) implemented in `pymc3` to generate samples from this posterior pdf, given data from each of the data sets defined in Table 1. We sample over the parameters LG mass $M_{\rm LG}$, the present-day MW–M31 halo separation r, log eccentricity $\ln(1-e)$, eccentric anomaly η, and the orbital plane orientation nuisance parameter α. Our adopted prior pdfs are defined in Table 2. For each data set, we run the sampler with four chains for 4000 tuning steps and 40,000 draws.

3. Results: Local Group Mass Estimates

We use a Bayesian implementation of a Timing Argument model to quantify the impact of the measured travel velocity of the MW disk from Petersen & Peñarrubia (2021) on the estimated mass of the LG, as well as other orbital parameters such as the distance between M31 and the MW. We compute convergence statistics using `Arviz` (Kumar et al. 2019) for all MCMC runs and find that the maximum Gelman–Rubin convergence statistic is $\leqslant 1.01$ for all parameters and each data set (Gelman & Rubin 1992). The mean inferred parameter values and their 68% credible regions from the sampled posterior pdfs for each data set are presented in Table 3. These results are also shown in Figure 2, again displaying the 68% credible regions of the LG mass, $M_{\rm LG}$, and eccentricity, e (lower-left panel). The upper-left panel shows the marginal posterior pdfs over LG mass for each of the data sets (histogram curves) and with 68% credible regions plotted for two prior LG mass measurements (gray shaded bands). We note that these values are for reference only, as we currently do not account for other known sources of bias in the TA model—such as a cosmological constant or cosmic bias—that may yield more accurate values.

Table 3
Mean Inferred Parameter Values and the 68% Credible Region of the Sampled Posterior Region for Each Data Set

Parameter	vdMG08 Dist. + HST PM	Cepheid Dist. + Gaia PM	Cepheid Dist. + HST PM
$M_{\rm LG}$	$3.98^{+0.6}_{-0.5}$	$4.54^{+0.8}_{-0.6}$	$4.05^{+0.5}_{-0.3}$
e	$0.92^{+0.1}_{-0.1}$	$0.84^{+0.1}_{-0.1}$	$0.92^{+0.1}_{-0.1}$
r	$777.72^{+36.6}_{-36.0}$	$765.17^{+10.9}_{-10.9}$	$765.44^{+10.8}_{-10.9}$
η	$-2.14^{+0.05}_{-0.04}$	$-2.08^{+0.04}_{-0.04}$	$-2.11^{+0.03}_{-0.03}$
α	$2.97^{+0.8}_{-0.8}$	$1.42^{+0.6}_{-0.5}$	$2.96^{+0.8}_{-0.8}$

Note. Here, $M_{\rm LG}$ is the mass of the Local Group, e is the eccentricity of the MW–M31 orbit, r is the distance between the centers of the MW and M31 halos, η is the eccentric anomaly (a proxy for the phase of the orbit), and α is a nuisance parameter representing the angle between the orbital plane of MW–M31 and the tangent plane located at the sky position of M31 as seen from the center of the MW disk.

We find that the addition of the travel velocity of the MW disk systematically decreases the inferred LG mass and eccentricity of the orbit compared to models that do not include the travel velocity of the MW disk. We also find that the inferred mass is larger and the LG orbit is less eccentric when using the (larger) Gaia proper motion of M31. For all data sets, the eccentricity of the decreases by ∼3%–5%. However, we find that the inferred orbital eccentricity is consistent with a radial orbit.

Figure 3 gives a summary of our key results, showing the behavior of the inferred LG mass and eccentricity as a function of the travel velocity. As the travel velocity increases from $\boldsymbol{v}_{\rm travel} = 0$ to $\boldsymbol{v}_{\rm travel} = 32 \pm 4$ km s^{-1}, shown by the vertical black line and gray shaded regions, the mass and eccentricity both decrease, with the effect on the mass drastically changing by up to $\sim 0.5 \times 10^{12}\ M_\odot$ and the MW–M31 orbit becoming more circular.

4. Discussion

4.1. Comparing Recent Measurements of the Local Group Mass

There have been two primary pathways toward measuring the mass of the LG: measure the masses of MW and M31 individually and add them, or go after the total mass directly with LV dynamics, the Timing Argument, or cosmological simulations.

Historically, the total mass estimates have been much larger than the sum of the individual MW and M31 masses: typical total LG masses are upwards of $4 \times 10^{12}\ M_\odot$, while the sum of independent MW+M31 mass measures result in a total mass closer to $2\text{–}2.5 \times 10^{12}\ M_\odot$, as can be seen in the collection of previous mass estimates for the LG, M31, and the MW in Table 4. It is not surprising that there are many discrepancies between the total and summed values of the LG mass, since

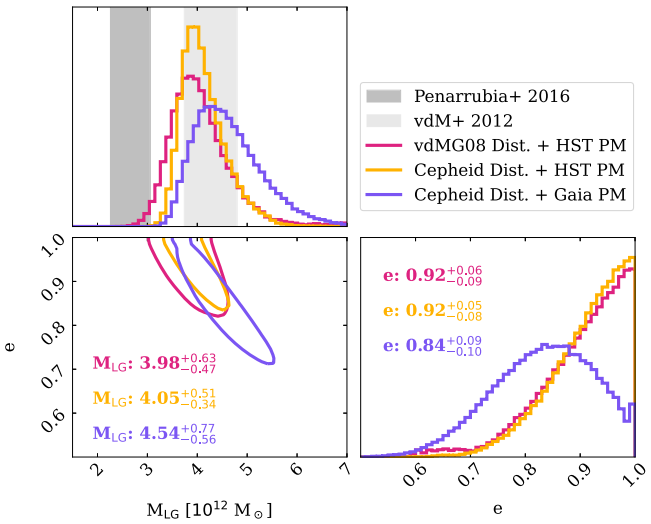

Figure 2. Sixty-eight percent credible regions of sampled posterior distributions with three observational data sets for a subset of our model parameters: the total mass of the Local Group (M_{LG}) and the eccentricity of the orbit of M31 about a fixed MW (e). Mean masses (in units of 10^{12} $M_\odot$) and eccentricities are reported in the bottom-left and bottom-right panels along with the 68% credible region for each data set. The shaded regions in the upper-left panel are the 68% credible region mass estimates of previous TA studies from van der Marel et al. (2012) and Peñarrubia et al. (2016). The more radial orbit implied by the van der Marel et al. (2012) HST proper motions leads to a lower inferred M_{LG} and a higher eccentricity, while the larger Gaia proper motions of Salomon et al. (2021) yield a more circular orbit, and thus a lower-eccentricity and higher-mass system.

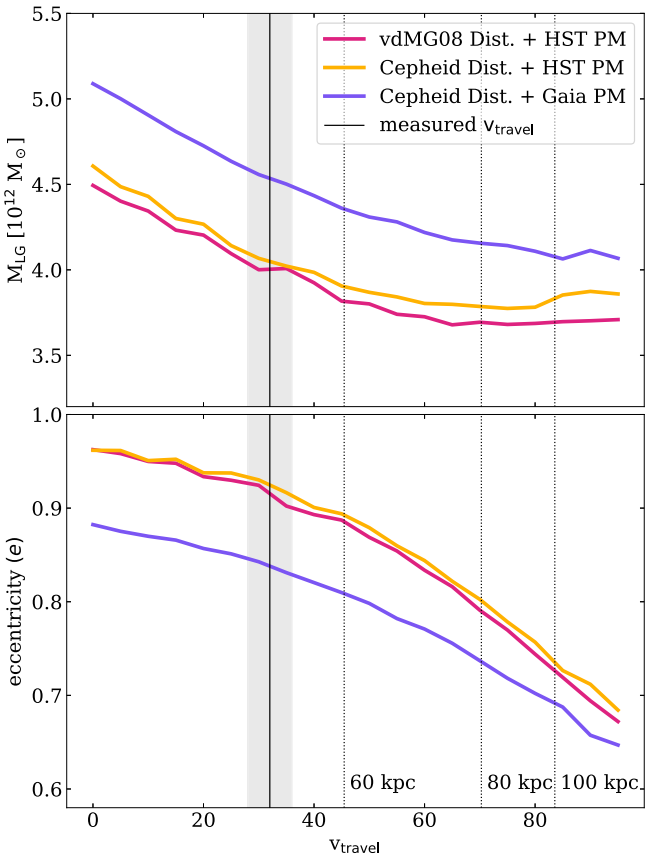

Figure 3. Mean inferred Local Group (LG) mass (top) and eccentricity (bottom) as a function of travel velocity magnitude of the MW disk. The larger Gaia proper motions (purple) lead to higher transverse motion and thus higher mass and a less eccentric orbit than either of the HST proper-motion data sets (pink and yellow), though each data set displays the same general trend with increasing travel velocity. The solid vertical line and accompanying shaded region represent the median and 67% confidence interval of the travel velocity measured by Petersen & Peñarrubia (2021) of $v_{travel} = 32 \pm 4$ km s^{-1}. The dotted vertical lines represent simulated travel velocities for stellar tracers at different distances in Garavito-Camargo et al. (2021). The inclusion of the travel velocity of the MW disk systematically lowers the inferred mass and eccentricity of the LG regardless of observational data set. A larger measured travel velocity will yield a lower mass, less radial LG.

MW+M31 (i.e., individual summed) mass estimates often cannot measure the full extent of the distribution of dark matter within each galaxy, let alone in the LG, and thus must extrapolate in regions where there may be large uncertainties.

There have been a few exceptions in the trend of high total mass measurements, namely in Diaz et al. (2014) and Peñarrubia et al. (2016). Diaz et al. (2014) utilize the fact that the LG momentum should balance to zero in the frame of the LG barycenter to determine the total mass of the LG, as well as the mass ratio between M31 and the MW. Using the LG barycenter, indicated by a set of 17 LG satellites at >350 kpc from the MW and M31, and the velocities of M31 and the MW with respect to the barycenter, they found a LG mass of $2.5 \pm 0.4 \times 10^{12}$ $M_\odot$, and a mass ratio $M_{M31}/M_{MW} > 2.29$. The impact of the LMC and M33 are absorbed by assuming they contribute to the masses of their host galaxies. However, the recent measurement of the MW travel velocity will change the measured barycenter and velocities of the MW, M31, and the LG satellites, though it is unclear how this would affect the total mass in their analysis.

Additionally, Peñarrubia et al. (2016) found a LG mass of $\sim 2.64 \pm 0.4 \times 10^{12}$ $M_\odot$, which is significantly lower than our findings, although this constraint combines the Timing Argument dynamics of the M31–MW system in addition to the observed kinematics of 35 LV galaxies. They parameterize the offset of the LMC+MW barycenter from a MW-only barycenter as a function of the mass ratio between the LMC and MW, and find that the LMC likely has ~25% of the mass of the MW halo, resulting in a large shift in the barycenter of the LMC+MW. The recovered mass using only the dynamics of the LV galaxies was quite low ($\sim 2 \times 10^{12}$ $M_\odot$), though including the Timing Argument dynamics of the MW–M31 system increased their recovered total mass to $\sim 2.64 \pm 0.4 \times 10^{12}$ $M_\odot$.

Our TA+v_{travel} LG mass estimates are consistent with a number of other recent studies that estimate the mass of the LG through dynamical methods. For example, we find agreement with the previous Timing Argument model of van der Marel et al. (2012), which found a total mass of $4.27 \pm 0.45 \times 10^{12}$ $M_\odot$ (neglecting for cosmic bias and scatter) using the same values for the distance and velocity of M31 as in our vdMG08 Dist. + HST PM data set.

In two N-body cosmological simulations, Millenium-WMAP7 and MilleniumII, Zhai et al. (2020) identified pairs of stellar analogs to the MW and M31, then applied a series of kinematic cuts on the separation, isolation, and velocities of the pair to determine LG analogs. They find stellar and dynamical LG analogs on mostly radial orbits have total masses of $4.4^{+2.4}_{-1.5} \times 10^{12}$ $M_\odot$, which is consistent with our findings for each data set. They also find that low-ellipticity orbits (where $v_{rad} \sim v_{tan}$), result in a higher LG mass, M31 mass, and MW mass, reporting $6.6^{+2.7}_{-1.5} \times 10^{12}$ $M_\odot$, $3.8^{+2.8}_{-1.8} \times 10^{12}$ $M_\odot$, and $2.5^{+2.2}_{-1.4} \times 10^{12}$ $M_\odot$, respectively. We find that the ellipticity of

Table 4
A Collection of Discussed Previous Mass Measurements from LG Dynamics Focusing on Previous Timing Argument Results

Mass	Method	Result ($10^{12}\,M_\odot$)	Citation
$M_{\rm LG}$	TA	3.6	Lynden-Bell (1981)
	TA (radial + cosmo sim calibration)	5.27	Li & White (2008)
	TA only	4.27 ± 0.45	van der Marel et al. (2012)
	TA (3D + cosmic bias and scatter)	4.93 ± 1.63	van der Marel et al. 2012
	Local Group (LG) dynamics	2.5 ± 0.4	Diaz et al. (2014)
	Local Volume galaxies + TA + Λ	2.64 ± 0.4	Peñarrubia et al. (2016)
	Machine learning	4.9 ± 0.8	McLeod et al. (2017)
	Machine learning (+large M31 transverse motion)	3.6 ± 0.3	McLeod et al. (2017)
	Cosmological sims	$4.4^{+2.4}_{-1.5}$	Zhai et al. (2020)
	Cosmological sims (likelihood-free inference)	$4.6^{+2.3}_{-1.8}$	Lemos et al. (2021)
	TA + Λ + cosmological sims	$4.75^{+2.22}_{-2.41}$	Hartl & Strigari (2022)
	TA + Λ + LMC	$5.6^{+1.6}_{-1.2}$	Benisty et al. (2022)
	TA + Λ + cosmic biad + LMC	$3.4^{+1.4}_{-1.1}$	Benisty et al. (2022)
	TA + $v_{\rm travel}$ (Cepheid + HST)	$4.0^{+0.5}_{-0.3}$	Chamberlain et al. (2022; this work)
	TA + $v_{\rm travel}$ (Cepheid + Gaia)	$4.5^{+0.8}_{-0.6}$	Chamberlain et al. (2022; this work)
$M_{\rm M31}$	Kinematics of M31 sats	1.4 ± 0.4 (<300 kpc)	Watkins et al. (2010)
	Giant Stellar Stream	$2.00^{+0.52}_{-0.41}$	Fardal et al. (2013)
	LG dynamics	1.7 ± 0.3	Diaz et al. (2014)
	Local Hubble Flow	1.33 ± 0.4	Peñarrubia et al. (2016)
	M31 orbital ang. mom.	$1.37^{+1.39}_{-0.75}$	Patel et al. (2017a)
	Cosmological sims	$1.0 - 2.0$	Carlesi et al. (2017)
	Cosmological sims	$2.5^{+1.3}_{-1.1}$	Zhai et al. (2020)
	Machine learning	$2.3 - 2.5$	Villanueva-Domingo et al. (2021)
	Machine learning (+ velocity information)	2.2–2.5	Villanueva-Domingo et al. (2021)
$M_{\rm MW}$	Kinematics of LG sats	1.4 ± 0.3 (<300 kpc)	Watkins et al. (2010)
	LG dynamics	0.8 ± 0.5	Diaz et al. (2014)
	Local Hubble Flow	1.04 ± 0.26	Peñarrubia et al. (2016)
	LMC orbital ang. mom.	$1.02^{+0.77}_{-0.55}$	Patel et al. (2017a)
	Cosmological sims	$0.6 - 0.8$	Carlesi et al. (2017)
	MW sats	$0.96^{+0.29}_{-0.28}$	Patel et al. (2018)
	Cosmological sims	$1.5^{+1.4}_{-0.7}$	Zhai et al. (2020)
	Machine learning	1.0–1.3	Villanueva-Domingo et al. (2021)
	Machine learning (+ velocity information)	2.3–2.6	Villanueva-Domingo et al. (2021)

the orbit decreases dramatically with larger travel velocities; however, in contradiction to Zhai et al. (2020), we find that this leads to a lower total LG mass.

Additionally, Benisty et al. (2022) recently modeled the contribution of the LMC-induced shift in the barycenter of the MW and used the Timing Argument to place constraints on the LG mass while removing the impact of the LMC. More specifically, they estimate the contribution of the reflex motion of the MW disk to the observed velocity vector of M31 by modeling the orbital history of the MW–M31 system and the MW+LMC–M31 system. The impact of the LMC on the mass measurements of the LG thus depend on the orbital and mass models of the LMC about the MW. This is in contrast to our work, which need make no assumption about the mass of the LMC, its orbital history, or the merger history of the MW. Upon implementing the Timing Argument, including a cosmological constant, and removing the LMC-induced reflex motion, they find a LG mass of $5.6^{+1.6}_{-1.2} \times 10^{12}\,M_\odot$, which is roughly 25% larger than our findings, and that accounting for cosmic bias and scatter lowers the mass by an additional 40% to $3.4^{+1.4}_{-1.1} \times 10^{12}\,M_\odot$, 25% lower than our findings. However, they find that, in general, inclusion of the motion of the MW disk due to the interaction with the LMC lowers the LG mass by ∼10%, which is consistent with our finding of a reduction in the total LG mass by ∼10%–12%.

A notable difference between this study and Benisty et al. (2022) is the method by which the reflex motion of the MW disk is accounted for. Rather than relying on accurately simulating the reflex motion of the disk, we let the travel velocity of the MW disk introduce a coordinate transformation (boost) of the measured velocity vectors of M31, and fit for the model parameters given the observable data. This method allows us to avoid model uncertainties in the mass profiles of each galaxy in the orbital models of the interaction between the MW, M31, and the LMC. Additionally, using the measured travel velocity also allows us to innately account for possible additional contributions to the present-day, instantaneous travel velocity induced by the extensive merger history of the MW in a robust way, without the need to simulate the entire interaction history.

4.2. Additional Sources of Bias to the Timing Argument

Given the simplicity of the Timing Argument dynamical model—in particular, the assumption that the MW and M31 are point masses with constant masses—it is reasonable to wonder whether this methodology provides unbiased estimates of the true LG mass. An early study of a dark-matter-only cosmological simulation found that the Timing Argument applied to pairs of galaxies did provide unbiased estimates of the sum of masses of the pairs (Li & White 2008). However,

more recently it was found that conditioning on LG analogs with similar radial and tangential velocities to the MW and M31 leads to slightly biased (overestimated) inferred total masses of those systems (González et al. 2014; Hartl & Strigari 2022). In this work, we do not attempt to "correct" our inferred LG masses for this cosmic bias effect, because it is unclear whether cosmological simulations accurately reproduce the detailed properties of LG systems. Accounting for this effect would likely lower our reported LG mass measurements. However, as we have shown, the existence of a reflex motion of the MW disk as a response to the MW's interaction with its satellite population decreases is an additional perturbation to the TA that must be considered in future studies alongside cosmic bias and a cosmological constant.

4.3. Impact of Travel Velocity on Inferred Dynamics of the Local Group

The existence of the travel velocity of the MW disk results in measurable differences in the estimated mass of the LG through the Timing Argument. These results are consistent with Erkal et al. (2020), who find that neglecting the LMC-induced reflex motion of the MW can result in masses that are overestimated by up to 50%. As shown in our results above, neglecting this motion at its currently measured value of $\boldsymbol{v}_{\rm travel} = 32 \pm 4$ km s^{-1} (Petersen & Peñarrubia 2021) leads to LG masses that are overestimated by ∼30%. However, both the magnitude and *direction* of the travel velocity are directly tied to the inferred mass of the LG. As it is currently measured, the (highest likelihood) direction of $\boldsymbol{v}_{\rm travel}$ is ∼60° from the sky position of M31, meaning that the travel velocity impacts the conversion of both M31's observed proper motion and radial velocity from a heliocentric reference frame to the "outer halo" reference frame used above. At fixed magnitude, if the true apex of the travel velocity motion is closer (farther) to M31's sky position, it would primarily affect the radial velocity (proper motions).

There is reason to believe that the recently measured MW disk travel velocity could be a lower bound on the true value, which could be up to a factor of ∼2–3 higher than the currently measured value. Using an idealized simulation of an equilibrium dark matter halo that has a recent merger with an LMC-like halo, Garavito-Camargo et al. (2021) showed that stellar halo tracers at different distances from the MW disk center may result in different measured travel velocities. While this simulation does not span previous mergers in the MW's history, it gives a good first-order approximation of what we may expect to observe. At fixed apex direction, a larger travel velocity would correspond to a lower inferred LG mass. Figure 3 shows the effect of increasing the measured travel velocity magnitude up to these predicted values and the impact on the inferred mass of the LG for each of the data sets used in this work (see Section 2.2). The vertical lines in this figure show the LMC-induced travel velocities that are predicted for three tracer distances in simulations from Garavito-Camargo et al. (2021). Thus, future measurements of the travel velocity of the disk that use tracers at larger distance around the MW stellar halo will likely lead to a lower inferred LG mass. We note again that the value of the eccentricity is derived assuming a matter-only universe (i.e., we neglect other cosmological effects in the orbit computation, as discussed above).

4.4. Improved M_{LG} Constraints from Future Observations

The biggest source of uncertainty in our empirically inferred LG mass, $M_{\rm LG}$, currently comes from the proper-motion measurements, which have signal-to-noise ratios of just 3–4. Future data releases from the Gaia Mission (Gaia Collaboration et al. 2016) will lead to more precise mean proper motions of M31 and thus more precise Timing Argument constraints on the LG mass. For example, between Gaia eDR3 and the end of the extended (10 yr) mission, the expected individual-source proper-motion precision improvement for a $G = 20$ source (i.e., an upper-giant-branch star in M31) is a factor of ∼6. Naïvely scaling the proper-motion uncertainties of M31 as measured with Gaia (Salomon et al. 2021) by a factor of 6 leads to a ∼2× improvement in the $M_{\rm LG}$ precision. Of course, the true improvement of the mean M31 proper motion with improved individual source kinematics could be even better than linear because more sources will be detected and usable in the measurement.

4.5. Reflex Motion of M31

While M31 has a massive satellite (M33) of comparable mass ratio to the MW–LMC system, we do not expect there to be a significant reflex velocity of M31's disk relative to its equivalent outer halo reference frame. Recent work predicts that M33 is likely on first infall into the M31 halo and has a much larger orbital pericenter than the MCs (e.g., Patel et al. 2017b). Additionally, M31 has likely experienced other significant mergers, as evidenced by the double nucleus and Giant Southern Stream (e.g., Ibata et al. 2001; Font et al. 2006), but these were likely lower mass-ratio mergers (e.g., Gilbert et al. 2019; Milošević et al. 2022) and thus will have less of an impact on the bulk motion of the M31 disk. Given current knowledge of the M31 system and uncertainties in the orbital histories of its most massive satellites, here we neglect the reflex motion of the M31 disk. However, a measurement or upper limit on the M31 disk travel velocity would enable further unbiased constraints on the LG mass.

4.6. MW and M31 Individual Masses

Reconciling techniques that compute the LG mass from the summed MW+M31 mass and from the Timing Argument is not straightforward, but the two approaches are complimentary. Future measurements of the travel velocity at large Galactocentric distances will likely exceed current measurements (see Section 4.3), which directly implies a lower LG mass and may improve agreement between these two general methods for estimating the LG mass. Since constraints on the MW mass consistently find a mass of $\sim 10^{12}\ M_{\odot}$, if not slightly higher (see, for reference, Table 4), our mass limits from the Timing Argument may begin to place meaningful upper limits on the mass of the M31 system.

4.7. The Circularity of the MW–M31 Orbit

The Timing Argument is highly sensitive to the tangential motion of M31, and larger proper motions will generically lead to lower eccentricities and higher inferred LG masses. Recent Gaia proper motions of M31 suggest the orbit of MW–M31 is less radial than previously believed (van der Marel et al. 2019; Salomon et al. 2021). Neglecting the travel velocity ($\boldsymbol{v}_{\rm travel} = 0$ in the above plots), we find that proper motions from HST (van

der Marel et al. 2012) are consistent with a highly radial orbit $e \sim 0.96$, while proper motions from Gaia (Salomon et al. 2021) result in a slightly lower eccentricity of $e \sim 0.88$. As seen in Figure 3, we find that as the travel velocity increases, the inferred eccentricity of the MW–M31 orbit decreases. However, contrary to expectations, we find that the inferred LG mass *also* decreases. This implies that the velocity contribution to the relative and transverse velocity of M31 is dominant to the change in eccentricity.

Additionally, studies of the Bolshoi *N*-body cosmological simulation by Forero-Romero et al. (2013) find that typical LG analogs, when selected via mass and isolation criteria, do not have completely radial orbits. As with studies that measure a higher transverse velocity for M31, and thus a slightly less radial orbit (van der Marel et al. 2019; Salomon et al. 2021), we find that the decrease in the eccentricity due to the measured travel velocity makes the LG less eccentric and, thus, more cosmologically typical.

5. Summary and Conclusions

Recent measurements of tracers in the outer MW stellar halo ($40 < r < 120$ kpc) by Petersen & Peñarrubia (2021) measure an instantaneous differential "travel velocity" of the MW disk compared to the outer stellar halo. The travel velocity has been inferred as primarily due to the response of the MW halo to the recent infall of the LMC (Erkal et al. 2019). In this work, we study the effect of the travel velocity on the inferred LG mass from the Timing Argument empirically for the first time. This allows us to avoid modeling uncertainties in the LMC orbital history and mass profile as well as uncertainties in the MW merger history.

We also consider three compilations of kinematic data for the distance and proper motion of M31, and find a decrease in the inferred mass compared to non-travel-velocity Timing Argument models . For each data set, as follows:[7]

1. For the vdMG08 Dist. + HST PM data set—the van der Marel & Guhathakurta (2008) distance and HST proper-motion measurements (Sohn et al. 2012; van der Marel et al. 2012)—we find a LG mass of $M_{\rm LG} = 3.98^{+0.63}_{-0.47} \times 10^{12}\,M_\odot$ (including the measured travel velocity), and of $M_{\rm LG} = 4.49^{+0.47}_{-0.42} \times 10^{12}\,M_\odot$ when $\boldsymbol{v}_{\rm travel}$=0. Thus, the inclusion of the travel velocity decreases the inferred LG mass by 11.36%.
2. For the Cepheid Dist. + HST PM data set—an updated Cepheid distance measurement from Li et al. (2021) and the same HST PMs from above—we find a LG mass of $M_{\rm LG} = 4.05^{+0.51}_{-0.34} \times 10^{12}\,M_\odot$ (including the measured travel velocity), and of $M_{\rm LG} = 4.61^{+0.42}_{-0.22} \times 10^{12}\,M_\odot$ when $\boldsymbol{v}_{\rm travel}$=0. Thus, the inclusion of the travel velocity decreases the inferred LG mass by 12.01%.
3. For the Cepheid Dist. + Gaia PM data set—a combination of the more recent Cepheid distance and latest Gaia proper-motion measurements of M31 (Li et al. 2021; Salomon et al. 2021)—we find a LG mass of $M_{\rm LG} = 4.54^{+0.77}_{-0.56} \times 10^{12}\,M_\odot$ (including the measured travel velocity), and of $M_{\rm LG} = 5.09^{+0.72}_{-0.48} \times 10^{12}\,M_\odot$ when $\boldsymbol{v}_{\rm travel}$=0. Thus, the inclusion of the travel velocity decreases the inferred LG mass by 10.88%.

[7] Errors correspond to the 68% credible regions about the median LG mass from the MCMC sampled posterior pdfs of our model parameters.

Our conclusions can be summarized as follows:

1. The measured travel velocity of the MW disk directly implies a reduced LG mass from the Timing Argument. For the measured travel velocity of 32 ± 4 km s^{-1} from Petersen & Peñarrubia (2021), the inferred LG mass is ~10%–15% lower than a system with a static MW halo ($\boldsymbol{v}_{\rm travel} = 0$). Using the same distance and proper motions as in the Timing Argument model of van der Marel et al. (2012), we find that the inclusion of the travel velocity yields a reduction in the LG mass of $\sim 0.3 \times 10^{12}\,M_\odot$.
2. Higher travel velocity measurements will yield lower LG masses. Simulations (Garavito-Camargo et al. 2021) suggest that tracers at large Galactocentric distances (60–100 kpc) will yield larger measurements of the travel velocity. If the travel velocity is measured to be larger based on tracers at larger Galactocentric distances, this will result in a decrease in the inferred LG mass by an additional 5%–12%.
3. The inferred eccentricity of the MW–M31 orbit is decreased by 3%–5% when accounting for the measured travel velocity. With a larger measured travel velocity, the inferred MW–M31 orbit would be less radial. The inferred eccentricity decreases by up to ~50% for the largest travel velocities we consider ($\boldsymbol{v}_{\rm travel} = 100$ km s^{-1}) compared to the static MW-halo model ($\boldsymbol{v}_{\rm travel} = 0$). Less radial orbits are cosmologically preferred, thus the travel velocity makes the LG more cosmologically typical.
4. Improvements in M31 proper-motion measurements will improve Timing Argument mass precision. With future data releases from the Gaia Mission, we expect the proper-motion uncertainties to improve by a factor of ~2–3 for individual sources (and likely more for measurements of the mean proper motions of stellar systems and galaxies like M31). We artificially scaled the proper-motion errors in each data set and find an expected improvement in the uncertainty on the inferred LG mass by a factor of 2–2.5× (see Section 4.4 for more detail).

This study highlights the importance of improved dynamical measurements within the LV in the near future in order to accurately measure the dark matter content of our LG. It is critical to refine our measurements of the proper motion of M31 and to measure the travel velocity of the MW disk with stellar tracers at further Galactocentric distances. These endeavors will (1) further refine estimates of the mass of the LG, enabling studies to realistically place the LG in a cosmological context, and (2) permit measurements of the travel velocity induced by the infall of the LMC and other satellite galaxies relative to tracers at large Galactocentric distances, which will establish a firm measurement of the LG mass via the Timing Argument, and thereby place meaningful limits on the individual masses of the M31 and MW galaxy.

This project was started at the Big Apple Dynamics School (BADS) hosted by the Flatiron Institute 2021 July–August. We greatly benefitted from discussions with the other students who attended the BADS, and received helpful input from Kathryn Johnston (Columbia), Alex Riley (Texas A&M), and Martin Weinberg (University of Massachusetts at Amherst). K.C. would like to thank Ekta Patel for sharing a

collection of M31 mass measurements from the literature. This research made use of Astropy,[8] a community-developed core Python package for Astronomy (Astropy Collaboration et al. 2013, 2018). K.C. and G.B. are supported by NSF CAREER AST-1941096 and NASA ATP 17-ATP17-0006. M. S.P. acknowledges grant support from Segal ANR-19-CE31-0017 of the French Agence Nationale de la Recherche (https://secular-evolution.org).

Software: Arviz (Kumar et al. 2019), Astropy (Astropy Collaboration et al. 2013, 2018), gala (Price-Whelan 2017), IPython (Pérez & Granger 2007), matplotlib (Hunter 2007), numpy (Harris et al. 2020), pymc3 (Salvatier et al. 2016), scipy (Virtanen et al. 2020).

ORCID iDs

Katie Chamberlain https://orcid.org/0000-0001-8765-8670
Adrian M. Price-Whelan https://orcid.org/0000-0003-0872-7098
Gurtina Besla https://orcid.org/0000-0003-0715-2173
Emily C. Cunningham https://orcid.org/0000-0002-6993-0826
Nicolás Garavito-Camargo https://orcid.org/0000-0001-7107-1744
Michael S. Petersen https://orcid.org/0000-0003-1517-3935

References

Astropy Collaboration, Price-Whelan, A. M., Sipőcz, B. M., et al. 2018, AJ, 156, 123
Astropy Collaboration, Robitaille, T. P., Tollerud, E. J., et al. 2013, A&A, 558, A33
Benisty, D., Vasiliev, E., Evans, N. W., et al. 2022, ApJL, 928, L5
Bennett, M., & Bovy, J. 2019, MNRAS, 482, 1417
Besla, G., Patton, D. R., Stierwalt, S., et al. 2018, MNRAS, 480, 3376
Carlesi, E., Hoffman, Y., Sorce, J. G., & Gottlöber, S. 2017, MNRAS, 465, 4886
Conroy, C., Naidu, R. P., Garavito-Camargo, N., et al. 2021, Natur, 592, 534
Courteau, S., & van den Bergh, S. 1999, AJ, 118, 337
Cunningham, E. C., Garavito-Camargo, N., Deason, A. J., et al. 2020, ApJ, 898, 4
Deason, A. J., Erkal, D., Belokurov, V., et al. 2021, MNRAS, 501, 5964
Diaz, J. D., Koposov, S. E., Irwin, M., Belokurov, V., & Evans, N. W. 2014, MNRAS, 443, 1688
Dooley, G. A., Peter, A. H. G., Yang, T., et al. 2017, MNRAS, 471, 4894
Drimmel, R., & Poggio, E. 2018, RNAAS, 2, 210
Eadie, G., & Jurić, M. 2019, ApJ, 875, 159
Erkal, D., Belokurov, V., Laporte, C. F. P., et al. 2019, MNRAS, 487, 2685
Erkal, D., Belokurov, V. A., & Parkin, D. L. 2020, MNRAS, 498, 5574
Erkal, D., Deason, A. J., Belokurov, V., et al. 2021, MNRAS, 506, 2677
Fardal, M. A., Weinberg, M. D., Babul, A., et al. 2013, MNRAS, 434, 2779
Fillingham, S. P., Cooper, M. C., Boylan-Kolchin, M., et al. 2018, MNRAS, 477, 4491
Font, A. S., Johnston, K. V., Guhathakurta, P., Majewski, S. R., & Rich, R. M. 2006, AJ, 131, 1436
Forero-Romero, J. E., Hoffman, Y., Bustamante, S., Gottlöber, S., & Yepes, G. 2013, ApJL, 767, L5
Fritz, T. K., Di Cintio, A., Battaglia, G., Brook, C., & Taibi, S. 2020, MNRAS, 494, 5178
Gaia Collaboration, Prusti, T., de Bruijne, J. H. J., et al. 2016, A&A, 595, A1
Garavito-Camargo, N., Besla, G., Laporte, C. F. P., et al. 2019, ApJ, 884, 51
Garavito-Camargo, N., Besla, G., Laporte, C. F. P., et al. 2021, ApJ, 919, 109
Gravity Collaboration, Abuter, R., Amorim, A., et al. 2018, A&A, 615, L15
Garrison-Kimmel, S., Hopkins, P. F., Wetzel, A., et al. 2019a, MNRAS, 487, 1380
Garrison-Kimmel, S., Wetzel, A., Hopkins, P. F., et al. 2019b, MNRAS, 489, 4574
Gelman, A., & Rubin, D. B. 1992, StaSc, 7, 457
Gilbert, K. M., Kirby, E. N., Escala, I., et al. 2019, ApJ, 883, 128
Gómez, F. A., Besla, G., Carpintero, D. D., et al. 2015, ApJ, 802, 128
González, R. E., Kravtsov, A. V., & Gnedin, N. Y. 2014, ApJ, 793, 91
Harris, C. R., Millman, K. J., van der Walt, S. J., et al. 2020, Natur, 585, 357
Hartl, O. V., & Strigari, L. E. 2022, MNRAS, 511, 6193
Homan, M. D., & Gelman, A. 2014, J. Mach. Learn. Res., 15, 1593
Hunter, J. D. 2007, CSE, 9, 90
Ibata, R., Irwin, M., Lewis, G., Ferguson, A. M. N., & Tanvir, N. 2001, Natur, 412, 49
Jarosik, N., Bennett, C. L., Dunkley, J., et al. 2011, ApJS, 192, 14
Kahn, F. D., & Woltjer, L. 1959, ApJ, 130, 705
Kroeker, T. L., & Carlberg, R. G. 1991, ApJ, 376, 1
Kumar, R., Carroll, C., Hartikainen, A., & Martin, O. 2019, JOSS, 4, 1143
Laporte, C. F. P., Gómez, F. A., Besla, G., Johnston, K. V., & Garavito-Camargo, N. 2018a, MNRAS, 473, 1218
Laporte, C. F. P., Johnston, K. V., Gómez, F. A., Garavito-Camargo, N., & Besla, G. 2018b, MNRAS, 481, 286
Lemos, P., Jeffrey, N., Whiteway, L., et al. 2021, PhRvD, 103, 023009
Li, S., Riess, A. G., Busch, M. P., et al. 2021, ApJ, 920, 84
Li, Y.-S., & White, S. D. M. 2008, MNRAS, 384, 1459
Lynden-Bell, D. 1981, Obs, 101, 111
Marinacci, F., Grand, R. J. J., Pakmor, R., et al. 2017, MNRAS, 466, 3859
McLeod, M., Libeskind, N., Lahav, O., & Hoffman, Y. 2017, JCAP, 2017, 034
McMillan, P. J. 2011, MNRAS, 414, 2446
Milošević, S., Mićić, M., & Lewis, G. F. 2022, MNRAS, 511, 2868
Partridge, C., Lahav, O., & Hoffman, Y. 2013, MNRAS, 436, L45
Patel, E., Besla, G., & Mandel, K. 2017a, MNRAS, 468, 3428
Patel, E., Besla, G., Mandel, K., & Sohn, S. T. 2018, ApJ, 857, 78
Patel, E., Besla, G., & Sohn, S. T. 2017b, MNRAS, 464, 3825
Peebles, P. J. E. 2017, arXiv:1705.10683
Peñarrubia, J., & Fattahi, A. 2017, MNRAS, 468, 1300
Peñarrubia, J., Gómez, F. A., Besla, G., Erkal, D., & Ma, Y.-Z. 2016, MNRAS, 456, L54
Peñarrubia, J., Ma, Y.-Z., Walker, M. G., & McConnachie, A. 2014, MNRAS, 443, 2204
Pérez, F., & Granger, B. E. 2007, CSE, 9, 21
Petersen, M. S., & Peñarrubia, J. 2020, MNRAS, 494, L11
Petersen, M. S., & Peñarrubia, J. 2021, NatAs, 5, 251
Planck Collaboration, Aghanim, N., Akrami, Y., et al. 2020, A&A, 641, A6
Price-Whelan, A. M. 2017, JOSS, 2, 388
Putman, M. E., Zheng, Y., Price-Whelan, A. M., et al. 2021, ApJ, 913, 53
Salomon, J. B., Ibata, R., Reylé, C., et al. 2021, MNRAS, 507, 2592
Salvatier, J., Wieckiâ, T. V., & Fonnesbeck, C. 2016, PeerJ Comput. Sci., 2, e55
Sawala, T., McAlpine, S., Jasche, J., et al. 2022, MNRAS, 509, 1432
Schönrich, R., Binney, J., & Dehnen, W. 2010, MNRAS, 403, 1829
Sohn, S. T., Anderson, J., & van der Marel, R. P. 2012, ApJ, 753, 7
Tolstoy, E., Hill, V., & Tosi, M. 2009, ARA&A, 47, 371
van der Marel, R. P., Fardal, M., Besla, G., et al. 2012, ApJ, 753, 8
van der Marel, R. P., Fardal, M. A., Sohn, S. T., et al. 2019, ApJ, 872, 24
van der Marel, R. P., & Guhathakurta, P. 2008, ApJ, 678, 187
Villanueva-Domingo, P., Villaescusa-Navarro, F., Genel, S., et al. 2021, arXiv:2111.14874
Virtanen, P., Gommers, R., Oliphant, T. E., et al. 2020, NatMe, 17, 261
Wang, J., Hammer, F., & Yang, Y. 2022, MNRAS, 510, 2242
Watkins, L. L., Evans, N. W., & An, J. H. 2010, MNRAS, 406, 264
Zhai, M., Guo, Q., Zhao, G., Gu, Q., & Liu, A. 2020, ApJ, 890, 27

[8] http://www.astropy.org